A three-phase Eulerian–Lagrangian model to simulate mixing and oxygen transfer in activated sludge treatment

Chen, Boyang; Fraga, Bruño; Hemida, Hassan

DOI:
10.1016/j.ijmultiphaseflow.2023.104555

Document Version
Publisher's PDF, also known as Version of record

Citation for published version (Harvard):
Chen, B, Fraga, B & Hemida, H 2023, 'A three-phase Eulerian–Lagrangian model to simulate mixing and oxygen transfer in activated sludge treatment', *International Journal of Multiphase Flow*, vol. 168, 104555. https://doi.org/10.1016/j.ijmultiphaseflow.2023.104555

International Journal of Multiphase Flow 168 (2023) 104555

Contents lists available at ScienceDirect

International Journal of Multiphase Flow

journal homepage: www.elsevier.com/locate/ijmulflow

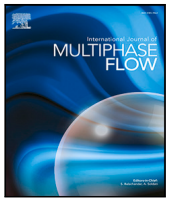

Review

A three-phase Eulerian–Lagrangian model to simulate mixing and oxygen transfer in activated sludge treatment

Boyang Chen *, Bruño Fraga, Hassan Hemida

School of Civil Engineering, University of Birmingham, Edgbaston, Birmingham B15 2TT, UK

ARTICLE INFO

Keywords:
Multiphase
Eulerian–Lagrangian
Large-eddy simulation
Oxygen transfer
Four-way coupling

ABSTRACT

We introduce a novel modelling tool for the activated sludge process (ASP) based on large-eddy simulation and multiphase Eulerian–Lagrangian coupling. Aeration-driven sludge activation is a key part of wastewater treatment and represents the vast majority of its energy consumption. Our model allows interaction among the liquid (wastewater), solid (sludge) and gas (air bubbles) phases, to provide insight on the fluid dynamics taking place during ASP. The model uses an Eulerian–Lagrangian point-particle algorithm that respects the discrete nature of both sludge flocs and air bubbles. Four-way coupling is implemented, where the interaction between solid particles is handled by a soft-sphere collision model. The analysis was focused on quantifying the Oxygen transfer from gas to liquid to solid, i.e., the conditions for aerobic bacteria activation. Such transfer is complex due to the dispersed nature of the gas and solid phases and the turbulent mixing occurring in the tank. Unlike box-modelling approaches, our three-dimensional model describes the evolution in space and time of the concentrations of these species and the Oxygen exchange, without a priori assumptions on the nature of the mixture. The model was validated versus experimental data using the interphase exchange of Oxygen as the key parameter, exhibiting in all cases an excellent agreement with measurements that qualitatively improves Eulerian–Eulerian approaches in five different tests. Subsequently our model was used to simulate a realistic scenario within the aeration basin of a wastewater plant and explore its results across a wide parameter range (aerator distribution, dissolved Oxygen levels, air flow rate, sludge size, bubble size). This allow us the explore the time evolution of the activation process and therefore test its performance versus the air flow rate injected (hence, energy). Our results indicate that the initial dissolved Oxygen levels within the basin (related to weather conditions and aeration frequency) are critical for sludge activation, with initial anoxic conditions being very taxing. For a given flow rate, bubble screens (i.e, more aerators) provide significantly better performance. Finally, we compare model estimations of bacterial Oxygen uptake with field data obtained from real-life ASP in wastewater plants, finding a good agreement. We therefore present to the community a reliable and extendable model that solves the fluid mechanics and the basic eco-hydraulics of the three-phase system encountered in wastewater plants, with minimal empirical inputs. This is a valuable and precise tool to test the operations and design of ASP and similar processes.

1. Introduction

The largest expense in wastewater treatment occurs in secondary treatment, particularly during activated sludge process (ASP) (Maktabifard et al., 2018). ASP is based on forced aeration to promote oxygen dissolution and dissemination within wastewater to facilitate microbial growth. In presence of sufficient oxygen, bacteria feed on organic material, forming larger flocs which settle and be efficiently removed in clarifiers. The process is designed to speed up the rate of decomposition in wastewater and improve the quality of effluent, and has been extensively applied in wastewater treatment plants around the world. Aeration accounts for 60% of the total energy consumption in ASP (Rieger et al., 2006; Fernández et al., 2011). There are two main types of aeration systems; surface aeration is implemented by installing turbines that inject air from the surface of the tank or basin. However, air diffusers that generate buoyant bubble plumes from the bottom of the tank are a much more popular alternative and generally considered more efficient (Sánchez-Monedero et al., 2008). Interestingly, albeit well-designed aeration systems are critical in an efficient and sustainable wastewater treatment, practitioners have been often forced

* Corresponding author.
E-mail address: b.fraga@bham.ac.uk (B. Chen).

https://doi.org/10.1016/j.ijmultiphaseflow.2023.104555
Received 26 October 2022; Received in revised form 8 June 2023; Accepted 20 June 2023
Available online 23 June 2023

to rely on empirical guidelines due to the lack of accurate modelling and design tools (Brouckaert and Buckley, 1999; Forster, 2003).

Experimental studies of ASP have typically focused on the biological characteristics of activated sludge and the dissolved oxygen (DO) concentration (Wilén and Balmér, 1999; Zhou et al., 2019). Some experimental research was carried out in a full-scale WWTP and continuously monitored the sludge concentration for months, exposing a remarkable influence of DO levels on the decomposition of organic material and the respiration of aerobic bacteria (Wilén and Balmér, 1998; Huang et al., 2019). In order to shorten the length of the experiments and test more efficiently the factors affecting the activated sludge's growth, Nowobilska-Majewska and Bugajski (2020) sampled the wastewater flowing into the aeration tank and measured the activated sludge concentration in a laboratory-scale tank. Overall, most experimental research on ASP focus on its general performance and does not explore in detail the complex multiphase flow and mass transfer that take place. In addition and for obvious reason, the number of design alternatives considered in the experiments is limited.

ASP involves a complex gas–liquid–solid three-phase flow consisting of buoyant bubble swarms and inertial solid particles within a liquid matrix, hence the physicochemical interaction among phases is key to their understanding. To quantify the biochemical process an accurate prediction of the DO distribution is required. DO concentration is heavily dependant on the turbulent mixing triggered by bubble plumes, the superficial transfer occurring at the individual bubbles and the adsorption by the sludge (Karpinska and Bridgeman, 2016). With a wide range of scales of motion implicated, it is necessary to predict accurately the shear layers generated by the individual plumes in order to describe the formation of recirculation cells within the aeration tank while simultaneously forecasting the in-plume dynamics in order to predict the entrainment of surrounding fluid and the generation of turbulent kinetic energy within the bubble swarm. It is important as well to characterise instantaneous flow properties since instabilities caused by dispersed phases (plumes and solid particles) and plume-wandering contribute to the mixing process, hence a non-transient modelling approach naturally tends to overlook these mechanisms. This and the fundamental role of multiphase turbulence justify the choice of large-eddy simulation (LES) to capture the instantaneous large-scale turbulent structures in the continuous liquid phase. LES-based simulations respect the anisotropic and transient nature of the dispersed phase (Fraga et al., 2016; Bridgeman, 2012) and have extensively applied to solve practical multiphase dispersed and particle-laden flows (Hu and Celik, 2008; Bini and Jones, 2008).

Regarding the dispersed gas and solid particle phases, the fundamental modelling choices are interface-solving methods, point-particle Eulerian–Lagrangian (PP-EL) schemes and continuous Eulerian–Eulerian (EE) models. Interface-solving models are extremely useful for fundamental research on multiphase flows, however when applied to particles such as air bubbles or suspended sludge flocs, their relatively small size compared to the length scales of the liquid matrix compels almost inexorably to use Direct Numerical Simulation. The resulting prohibitive computational cost limits therefore their application to flows of industrial interest (Yujie et al., 2012; Lu et al., 2005). EE approaches compute the dispersed phase on a continuous Eulerian framework, introducing a void/solid fraction variable to characterise the dispersed phase (Li et al., 2009). EE has been applied successfully to bubbly flows and particle-laden flows of practical interest (Fabregat et al., 2015; Dhotre et al., 2009; Sánchez et al., 2018; Terashima et al., 2009; Deen et al., 2004; Kartushinsky et al., 2016; Baker et al., 2020). By not considering the discrete nature of the particles, EE methods are very efficient and widely applicable, albeit within some limitations: they cannot naturally forecast the physics of the dispersed phase and its interaction with the continuous phase (e.g. liquid entrainment or particle settling Cantero et al., 2008); they cannot resolve naturally wall-particle interaction (Nasr-Azadani et al., 2013), and they struggle to simulate the effect of polydispersed distributions (Balachandar and Eaton, 2010) since the particle size is often modelled indirectly through single-value parameters such as the terminal velocity. PP-EL models do not rely on semiempirical parameters as the slip or settling velocity to induce the effect or particle size and particle Reynolds number Re_p, allowing modellers to implement organically polydispersed distributions (Sokolichin et al., 1997; Fraga et al., 2016; Fraga and Stoesser, 2016; Buwa et al., 2006; Chen et al., 2021); this of course comes at the expense of tracking individually a large number of particles, which is not always possible. Within this approach the dispersed phases are described as volumeless points in a Lagrangian framework, whereas the continuous one is calculated in an Eulerian framework fixed in space. The interaction between both phases is modelled depending on the particle size and concentration (Elghobashi, 1994). One-way coupling is employed where the advection of the carrier flow is dominant and the dispersed phase behaves in a nearly passive manner. With bubbly flows, due to the high density ratio between air bubbles and water, bubble buoyancy has a rather disruptive effect on the surrounding liquid, requiring a two-way coupling approach. For particle-laden flow with dense particle concentration, the particle-to-particle interaction must be also considered, hence four-way coupling (Hryb et al., 2009; Mehrabadi et al., 2018).

Several works have applied three-dimensional non-hydrostatic CFD coupled with biochemical kinetics to investigate ASP in wastewater treatment plants, including ASP. Le Moullec et al. (2010) explored the hydrodynamics in activated sludge reactors with a RANS-based Eulerian–Eulerian algorithm. The authors applied an established activated sludge model simulate the biochemical reactions and compared the results with experimental measurements of chemical oxygen demand (COD) and DO concentration. The simulation underpredicts the oxygen mass transfer due to assuming a steady flow field in the reactor. Xie et al. (2014) also used an EE-RANS model to study the velocity induced by the settling of sludge in a full-scale oxidation tank, where a empirical slip velocity was introduced to characterise the sludge's inertia. Sánchez et al. (2018) applied EE-RANS coupled with biokinetic models to investigate ASP and compared different strategies for distributing the air diffusers, showing that the efficiency of aeration system is sensitive to the number of blowers and air flow rate. Dapelo et al. (2015) studied sludge mixing of sludge in aeration tank using a RANS PP-EL model and assuming that there are no biochemical reactions during aeration. Air bubbles are modelled as Lagrangian markers, whereas sludge is solved in the Eulerian framework, incorporating rheology into the definition of the liquid's stress rate. The results prove the adequacy of such approach, despite some difficulties to capture the liquid velocities within the buoyant plumes. Karpinska et al. (2015) applied RANS (steady), URANS (unsteady) and LES to investigate the hydrodynamics of sludge in an oxidation ditch, with sludge being described as a suspension of solid particles and modelled by passive Lagrangian markers (one-way coupling). The residence time distribution was compared with experimental work, with LES showing a significantly better agreement over the others.

In this study, an in-house Navier–Stokes solver coupled with a point-particle Eulerian–Lagrangian algorithm (Fraga et al., 2016) is used to perform LES of the solid–liquid–gas three-phase flow encountered in activated sludge process (ASP). The solver's ability to predict gas–liquid flows has been successfully proven in the past regarding the liquid matrix velocity field, second-order statistics, plume integral properties and buoyancy-induced mixing (Fraga et al., 2016; Fraga and Stoesser, 2016; Chen et al., 2021). This work will further extend this model by solving simultaneously the gas–liquid–solid flow present in ASP, incorporating four-way coupling and bio-kinetics model for the oxygen transfer and consumption and validating these results. As discussed in the literature review, most computational fluid dynamics models of ASP are based on RANS, despite there being evidence of the adequacy of LES for this particular application due to the relevance of turbulent mixing and convection. The other source of limitations is the description of the dispersed gas and solid phases and their interactions. Our model

incorporates three fundamental novelties: (1) three-phase flow solver that combines LES with a PP-EL approach that respects the discrete nature of the dispersed phases (gas bubbles and sludge flocs) for the first time; (2) the sludge flocs are calculated on a Lagrangian framework that is four-way coupled, including particle–particle and particle–wall interactions; (3) we propose a methodology to track the whole cycle of oxygen across phases during the aeration process. Sludge rheology is considered by relating particle concentration fluid viscosity. Once validated, the model will be applied to ASP under real operating conditions. In addition to showcasing the model application, we investigate the influence of operating conditions, such as the setup of air diffusers or the initial DO distribution in the tank, to provide insight on the key working mechanisms of ASP.

2. An Eulerian-Lagrangian three-phase model

2.1. Continuous phase

The fluid flow is simulated using an enhanced version of the in-house LES-based Lagrangian particle-tracking algorithm BubLPT (Fraga et al., 2016), incorporated on the finite difference LES Navier–Stokes solver Hydro3D (Cevheri and Stoesser, 2018; Vui Chua et al., 2019). This code has been successfully applied to turbulent multiphase flows using LES (Fraga et al., 2016; Fraga and Stoesser, 2016; Chen et al., 2021) and DNS (Lai et al., 2018; Paul et al., 2022). The governing equations are the spatially filtered Navier–Stokes equations for turbulent, incompressible, three-dimensional flow,

$$\frac{\partial u_i}{\partial x_i} = 0 \tag{1}$$

$$\frac{\partial u_i}{\partial t} + \frac{\partial u_i u_j}{\partial x_j} = -\frac{\partial p}{\partial x_i} + 2\nu\frac{\partial (S_{ij})}{\partial x_j} - \frac{\partial \tau_{ij}}{\partial x_j} + \xi_i \qquad (for\ \ i = 1,2,3) \tag{2}$$

where u_i and x_i refer to the fluid velocity and position in the i Cartesian coordinate, respectively. t, p, ν and S_{ij} represent time, dynamic pressure, kinematic viscosity and strain rate tensor. The term τ is the sub-grid stress and is calculated by the turbulent viscosity ν_t ($\nu_t = (C_s\Delta)^2|\bar{s}|$, where Δ is the local grid size and $|\bar{s}|$ refers to the strain rate tensor), herein based on the Smagorinsky sub-grid scale (SGS) model with a constant coefficient $C_S = 0.1$. Finally, $\xi = \xi_s + \xi_g$ designates the source term that accounts for the contribution of the dispersed phases (inertial solid flocs ξ_s and buoyant gas bubbles ξ_g) to the flow's momentum. The time derivatives are discretised using a three-step Runge–Kutta algorithm and second-order central differencing scheme is applied to both convective and diffusive terms. The code is based on a predictor–corrector fractional step method with the solution of the Poisson pressure equation obtained through a multi-grid solver. The calculation procedure for every time step is implemented by Message Passing Interface (MPI) parallelisation (Ouro et al., 2019). In order to predict the fate of dissolved oxygen (DO) during aeration, the concentration field is modelled as passive scalar and solved by a filtered advection–diffusion transport Eq. (3), at each time step once the fluid field is calculated.

$$\frac{\partial [DO]}{\partial t} + u_i\frac{\partial [DO]}{\partial x_i} = (D + D_t)\frac{\partial^2 [DO]}{\partial x_i^2} \tag{3}$$

where $[DO]$ is the concentration of dissolved oxygen, $D_t = \nu_t/Sc_t$ is the sub-grid scale turbulent diffusivity and D is the molecular diffusivity. Sc_t represents the turbulent Schmidt number that has a value of 0.7 as adopted in similar studies (Ouro et al., 2018).

2.2. Dispersed phase: gas bubbles and sludge flocs

The dispersed phase is simulated using a Lagrangian Particle Tracking algorithm in which each particle is represented by a single volumeless point that moves across the domain detached from the computational grid, on Lagrangian coordinates. The multiphase flows analysed in the current work exhibit gas and solid volume fractions around 0.06% and 2.0%, respectively. Two-way coupling is adopted to calculate the dynamics of the gas phase and quantify its contribution to the carrier flow. The solid fraction, however, is nearly two orders of magnitude higher, and consequently a four-way coupling approach is needed to include particle-to-particle and particle-to-wall interactions. Such approach ensures that we can reproduce processes such as particle settlement and clustering. Based on the assumption that the dispersed phase (bubbles and solid particles, henceforth 'particles') are rigid and spherical, the motion of each one is computed by Newton's second law:

$$m_p\frac{\partial v_{p,i}}{\partial t} = F_{p,i} \qquad (for\ \ i = 1,2,3) \tag{4}$$

where m_p refers to the particle mass, $v_{p,i}$ is the particle's velocity in the Cartesian coordinate i, and $F_{p,i}$ refers to the sum of the interfacial force exerted by the liquid matrix on the particle. The forces acting on each particle, approximated by semi-empirical formulae, are buoyancy, fluid stress, added mass, drag and lift and their expressions are summarised in Table 1. The subscript p denotes particle, and therefore a variable described in the Lagrangian framework, as opposed to the Eulerian variables. More details on the performance of this model can be found in previous studies (Fraga et al., 2016; Fraga and Stoesser, 2016; Chen et al., 2021).

Table 1
Interfacial liquid forces acting on the particle in the PPL model.

Forces	Formulation
Buoyancy	$F_G = (m_p - m)g$
Fluid stress	$F_S = m\frac{Du}{Dt}$
Added mass	$F_A = -C_A m\frac{\partial}{\partial t}(u_p - u)$
Drag	$F_D = \frac{1}{2}C_D\rho A_{fr} \mid u_p - u \mid (u_p - u)$
Lift	$F_L = -C_L m_p(u_p - u)\times\omega$

A soft-sphere collision model firstly proposed by Cundall and Strack (1979) and developed by Capecelatro and Desjardins (2013) is applied to predict particle-to-particle and particle-to-wall interactions. This model is based on the assumption that the particles are spherical and models the interactions between particles as a mass–spring system. The collision force exerted on the particle a due to the collision with b is expressed as follow:

$$F^{col}_{n,a\to b} = \begin{cases} -\lambda\delta_{ab}n_{ab} - \eta u_{ab} & \text{if } d_{ab} < r_a + r_b + \gamma, \\ 0 & \text{else} \end{cases} \tag{5}$$

where n represents the normal component of collision force, γ denotes a stiffness parameter, η is the damping parameter, d_{ab} is the distance between the particles' centroids, δ_{ab} is the overlap between the two particles, λ defines the influence range, n_{ab} is the unit vector that links the particles' centroids and r is the radius of each particle. The relative normal velocity u_{ab} between two particles is defined as

$$u_{ab,n} = ((u_a - u_b)\cdot n_{ab})n_{ab} \tag{6}$$

The damping parameter η is used to account for energy dissipation, which can be solved with the coefficient of restitution e ($0 < e < 1$) and the effective mass $m_{ab} = (1/m_a + 1/m_b)^{-1}$,

$$\eta = -2ln e\frac{\sqrt{m_{ab}k}}{\pi^2 + (ln e)^2} \tag{7}$$

The stiffness parameter γ is applied to quantify the resistance force under deformation and is expressed as

$$\gamma = \frac{m_{ab}}{\tau_{col}^2}(\pi^2 + ln(e)^2) \tag{8}$$

where τ_{col} refers to the collision time accounting for the resolution of collision. And collisions with the wall are modelled by treating the wall as a particle with infinite mass and a radius of zero. In order to simulate the friction between two particles and the rotation of

particles, a simplified static fraction model suggested by Capecelatro and Desjardins (2013) is employed where the tangential displacement of two particles is neglected with high computational cost, the formula is as follow,

$$F^{col}_{t,a\to b} = -\mu_f \mid F^{col}_{n,a\to b} \mid t_{ab} \tag{9}$$

where t represents the tangential component of collision force, μ_f refers to friction coefficient and t_{ab} refers to a tangential unit vector that can be calculated by the relative tangential velocity,

$$t_{ab} = \frac{u_{ab} - u_{ab,n}}{\mid u_{ab} - u_{ab,n} \mid} \tag{10}$$

2.3. Sludge rheology and Lagrangian-to-Eulerian mapping

Activated sludge observes a rheological, non-Newtonian behaviour. Within our model the complex nature of sludge is represented as the interaction of a dispersed solid phase (sludge flocs) and water. The rheological characteristics of sludge manifest in the influence of the particle suspension on the surrounding liquid's viscosity. The Einstein equation (Eq. (11)) can be employed to relate the particle concentration to the overall viscosity of the mixture when the concentration of sludge is small and particle-to-particle interaction has no effect on the shear between liquids (Forster, 2002; Pryamitsyn and Ganesan, 2006; Eshtiaghi et al., 2013).

$$\nu_{sludge} = \nu_{water}(1 + 2.5\phi_{flocs}) \tag{11}$$

where ν_{sludge} and ν_{water} represent suspension and water kinematic viscosities, respectively, and ϕ_{flocs} refers to the local volume fraction of solid particles. The local volume fraction ϕ is evaluated over a cubic volume around each particle whose size depends on the particle diameter:

$$d_{cube} = d_p\gamma \tag{12}$$

where the minimum of the γ representing the ratio of cube size to particle size is equal to $(\pi/6)^{1/3}$ to ensure that the volume of cube is greater or equal to the volume of particle (Link et al., 2005). And the volume fraction in each cube ϕ_{cube} is calculated as follows,

$$\phi_{cube} = \frac{V_p}{V_{cube}} = \frac{\pi}{6\gamma^3} \tag{13}$$

which is used to compute the volume fraction of solid particles in cell j,

$$\phi^j_{cell} = 1 - \phi_{cube} \sum_{\forall i \in cell} \Phi^i_{cell} \tag{14}$$

where Φ^i_{cell} refers to the volume fraction of the cell j under the consideration of cube i. Thus, the viscosity of each Eulerian cell is updated in each time step based on Eq. (11) and the position of each Lagrangian solid particle (sludge).

2.4. Interphase oxygen transfer

There are two key processes in the inter-phase exchange of oxygen during ASP, the input of oxygen from air bubbles into the liquid matrix (DO generation) and the output of DO from liquid to sludge flocs as a result of the metabolism of aerobic bacteria present in the activated sludge (DO consumption). To simulate the oxygen exchange between the air bubbles and the liquid phase, the model developed by Darmana et al. (2005) is adopted. Within this model, the interphase mass transfer is driven by mass fraction gradients; the mass transfer rate of oxygen $\dot{m}_b$(mg/s) can be expressed as

$$\dot{m}_{DO} = Ek_l A_b \rho_l([DO]^*_l - [DO]_l) \tag{15}$$

where A_b is the surface area of the air bubble, k_l represents the mass transfer coefficient for oxygen (Motarjemi and Jameson, 1978) and E is a coefficient that considers the effect of chemical reactions on the mass transfer ratio; we assumed that such effect is negligible, hence $E = 1$. $[DO]^*_l$ and $[DO]_l$ refer to the mass fraction of oxygen at the gas–liquid interface and in the liquid phase respectively. The former is obtained from the oxygen mass fraction in the bubble $[O_2]_b$:

$$[DO]^*_l = \mathrm{H}[\mathrm{O}_2]_b \frac{\rho_b}{\rho_l} \tag{16}$$

where H represents the Henry constant accounting for the relationship between the gas concentration and liquid pressure; $H = 0.0032$ for oxygen in water at 25 Celsius (Sander, 2015).

Aerobic bacteria present in the sludge consume the DO in the tank during activation. DO consumption is strongly affected by microorganism and sludge concentration (Smith, 1963). ASP mainly consists of four phases: (1) aeration-driven mixing provides a homogeneous DO for sludge growth; (2) the organic matter in the wastewater is degraded, contributing to sludge's growth and high DO consumption rates; (3) DO consumption falls as organic matter concentration decreases and oxidised flocs settle; (4) aeration ends and DO levels continue to slowly decrease as the microbial metabolism in the settled sludge gradually reduces. Our model focuses on the first two phases, that are critical to depict accurately the efficiency of the aeration. To do so, we track the sludge concentration (ϕ_{flocs}) based on their particle fraction (to see more details about Eulerian–Lagrangian coupling please refer to 2.3), the DO concentration and calculate the oxygen uptake rate per unit of time (OUR) using the empirical model developed by Nowobilska-Majewska and Bugajski (2020) (Eq. (17)), under the assumption that bacterial concentration in the sludge is high enough not to act as a limiting factor.

$$OUR = 16.9492 - 0.0018\phi_{flocs} \tag{17}$$

The oxygen uptake is however limited by the DO concentration around the sludge flocs $\dot{m}_{l\to s} = min(OUR \cdot \Delta t, DO^*_s)$, where DO^*_s is the oxygen concentration at the liquid–solid interface.

3. Experimental validation of oxygen transfer in a bubble reactor

The ability of this mode to predict oxygen transfer is tested against the experimental measurements performed by McClure et al. (2018). The experiments were carried out in a 0.39 m diameter cylindrical pilot-scale column. The height of liquid is set to 1 m at the beginning of each experiment. The aerators consisted on symmetrically drilled 0.5 mm holes, forming a tree-like structure shown in Fig. 1. This system is located 0.135 m above the bottom of the reactor and has a 2.2% free area that is not covered by the aerators. The oxygen transfer rate is experimentally measured by adding sodium sulphite in the water and calculating the changes on sulphite concentration over time. More experimental details can be found in McClure et al. (2018).

Numerical simulations are carried out on an analogous setup to the experiment and its details are shown in Table 2. The boundary conditions for the dispersed phase are the prescription of gas velocities ranging between 0.14 and 0.28 m/s. Three mesh resolutions were tested and, unless indicated otherwise, the medium one (uniform, 10 mm) was adopted. Bubbles are released at the aerator's holes and they are removed from the computational domain once they reach the water surface. Boundary conditions for the continuous phase include the use of the no-slip boundary condition at all solid walls and the bottom of the tank and a rigid lid at the water surface with a free slip condition. The initial DO level in the reactor is zero, and the only source of oxygen and motion are the air bubbles. The DO concentration field across the reactor is integrated to quantify the total oxygen transfer.

Fig. 2 presents the numerical predictions and experimental measurements of oxygen transfer rate in the reactor for different gas flow rates. Fig. 2a shows the comparison of our simulations (rectangles) with experimental results (triangles) and EE-RANS simulations (circles) by McClure et al. (2018). The measurements include an experimental standard deviation bar which varies between a minimum of ±10% and

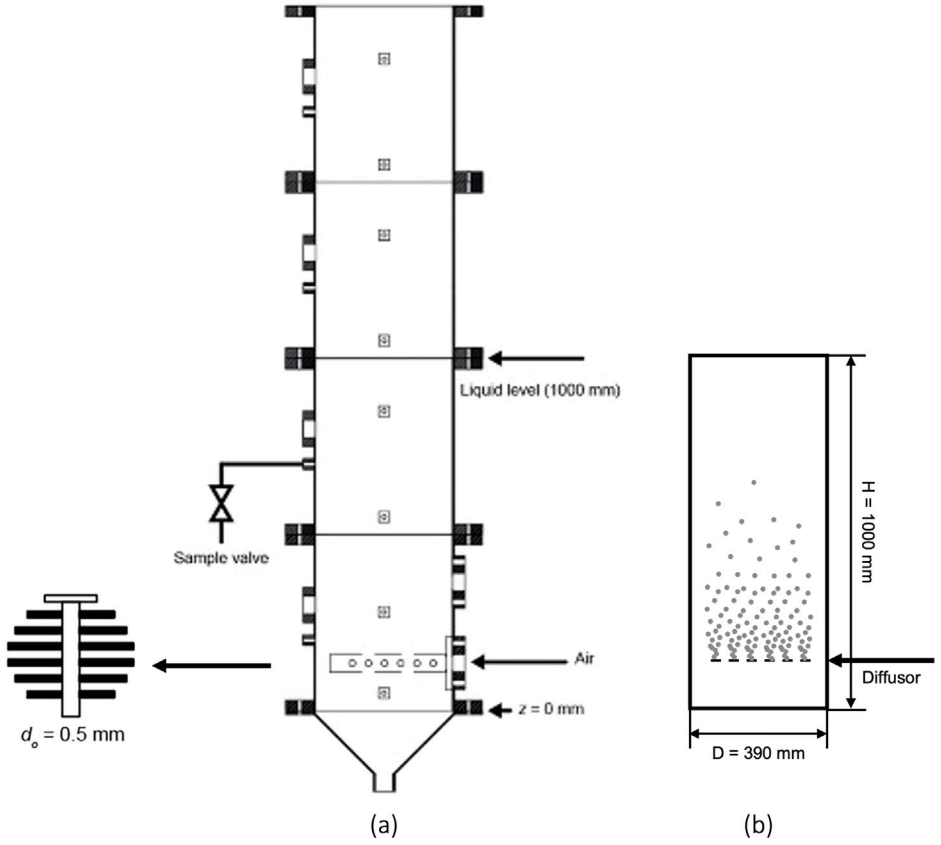

Fig. 1. Schematic diagram of bubble column: (a) Experimental layout (McClure et al., 2018); (b) Numerical setup.

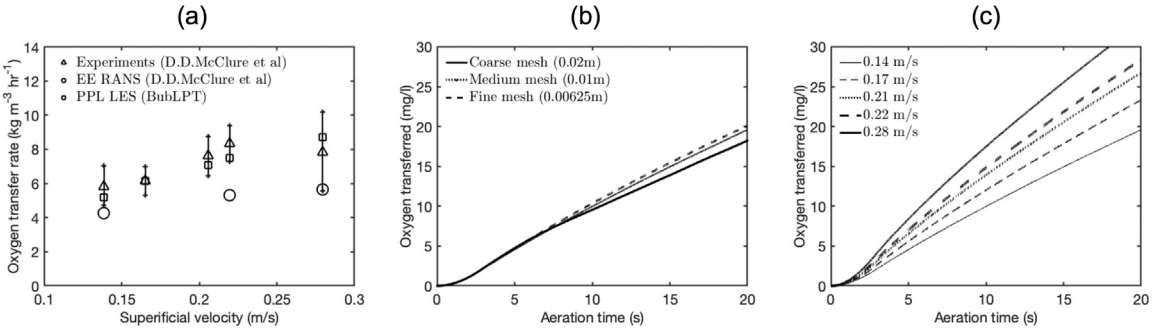

Fig. 2. Oxygen transfer rate for numerical and experimental data (McClure et al., 2018): (a) Experimental validation; (b) Mesh sensitivity analysis; (c) Sensitivity to superficial velocity.

Table 2
Numerical setup for the bubble reactor.

Parameters	Value	Unit
Bubble size	5.0	mm
Oxygen content in bubble	21	%
Mass transfer coefficient for oxygen	0.0004	m/s
Superficial velocity	0.14 to 0.28	m/s
Density of liquid	1040	kg/m^3
Density of air	1.4	kg/m^3
Mesh sizes	6.25, 10 and 20	mm
Time step	0.001	s

a maximum of ±20%, which occurs at the highest superficial velocity. Our numerical predictions always fall within the experimental margin of error, and show a consistent agreement throughout the whole parameter range. The results also suggest that our PP-LES model offers better predictions than the EE-RANS. This can be attributed to three fundamental aspects: (i) solving the larger scales of motion that interviene in instantaneous turbulent mixing; (ii) RANS is necessarily more reliant on turbulence closures, which have proved to be particularly inconsistent in the prediction of bubble-induced turbulence (Magolan et al., 2019); (iii) PP-LES is capable of simulating entrainment and detrainment of liquid within the plume minimising semi-empirical parametrisation. Fig. 2b reveals the time evolution of the oxygen concentration transferred with 0.14 m/s superficial velocity for the three grid resolutions. The results show a remarkable degree of convergence between the medium and finer meshes, whereas the coarser one deviates after 13 s of aeration, underpredicting the final transfer rate by 10%. Fig. 2c also shows the oxygen transferred versus time for all superficial air velocities. The oxygen transfer rate in Fig. 2a is obtained from the mean slope of these curves.

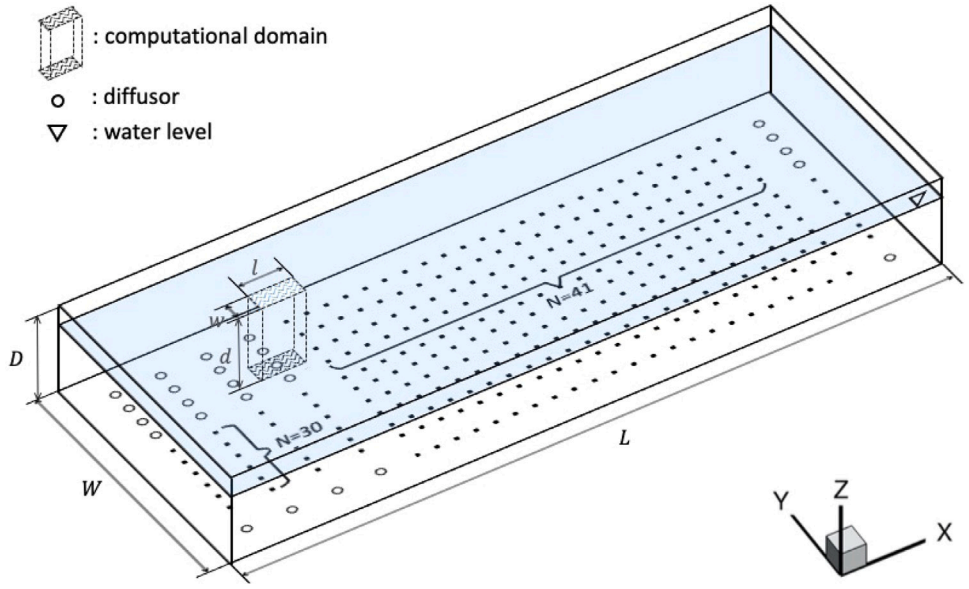

Fig. 3. Schematic diagram of an ASP basin: L, length of actual tank; W, width of actual tank; D, depth of actual tank; l, length of numerical domain; w, width of numerical domain; d, depth of numerical domain, N, total number of diffusers in horizontal or vertical direction of the tank.

4. ASP simulation under operation conditions

The LES-based ASP model is tested in a series of three-phase flow simulations that mimic the setup of an aeration basin in a real-life wastewater facility in the UK.

Fig. 3 shows our computational domain in the context of a real-size aeration basin for ASP in a wastewater treatment plant. The width/length ratio, depth and air blower distribution and spacing replicate a real basin in a wastewater treatment plant during normal operation. The tank's depth is 5 m and the average water level is 4 m. The diffusers have a diameter of 20 cm and are located 30 cm above the bottom of the tank. Since the distribution of aeratorns within the basin is symmetrical, we can assume a repetition of flow patterns around each diffuser, save for the ones by the walls. Hence, the computational domain described in Fig. 3 is a $1 \times 0.5 \times 4$ m box that replicates the flow surrounding a single diffuser located at a certain distance from the wall; periodic boundary conditions are applied to simulate the effect of the identical nearby aerators. The numerical setup is summarised in Table 3; all parameters correspond to normal operation values in real ASP facilities in the UK. Sludge concentration is chosen as 3400 mg/l falling within the reported range of real sludge in ASP facilities in the UK (3300 to 4500). To provide the amount of sludge required, 10^5 Lagrangian particles were used only for the sludge flocs. The air flow rate is calculated as a single diffuser's fraction within the total air conveyed into a real tank (approx. 180,000 l/min), which is approx. 40 l/min (i.e., 10^4 bubbles per second). All the lateral boundaries are periodic both for the Eulerian and Lagrangian phases. The solid particles collide with the bottom of tank, where they settle and accumulate. The top boundary is modelled as a rigid lid in which bubbles are removed from the computational domain once surpassed. Anoxic initial conditions are assumed, and the only sources of DO are the bubbles and molecular diffusion at the tank's free surface.

Fig. 4 illustrates how the dissolved oxygen (DO) is transferred from air bubbles to water. For clarity, the solid fraction is not shown in this figure, despite being part of the simulation. Based on prior insight on buoyancy-induced mixing (Chen et al., 2021), two aerator configurations were chosen and tested: (1) a single plume design that corresponds to the configuration depicted in Fig. 3, where the diffuser separation is 50 cm (Fig. 4a–b), (2) a screen-like design that distributes the same air flow rate over 5 diffusers separated 20 cm from each other (Fig. 4c–d). The total air flow rate is the same for both cases. The blowers are located along the central spanwise plane. The results show the early development – 7.5 s into the simulation – of DO concentration (a and c) and air bubbles, colour-coded by their oxygen fraction (b and d). The bubble O_2 level at release is 23%, and decreases as they rise and transfer it to the initially anoxic water. Fig. 4a and b show the bubble swarm rising up as it overcomes the water's inertia, resulting in the characteristic mushroom-shaped plume. The bubbles on top of the plume and, particularly, those that got trapped in the lateral recirculation, have transferred a significant amount of Oxygen (up to 20%), whereas the ones in the centre of the plume rise faster and have less exposure to the liquid. The bubble screen increases the exposure of all bubbles to the liquid matrix, avoiding the shielding effect. Since each individual diffuser in the screen releases 20% of the single plume's flow rate, the buoyant momentum is lower and the bubbles rise more slowly and homogeneously. The plumes forming the bubble screen loose their individual structure and form an unified swarm from $Z = 1.4$ m on. The higher residence time and more homogeneous mixing make the O_2 transfer to the liquid with the bubble screen more gradual and, overall, more effective. However, a sensor floating near the surface would detect a raise in DO levels much quicker in a single plume configuration.

Table 3
Numerical parameters for the ASP simulation (parts are Lagrangian particles).

Parameter	Value
Sludge concentration	3400 mg/l (10^5 parts)
Sludge density	1015 kg/m^3
Sludge floc size	4.0 mm
Air flow rate	40 l/min (10^4 part/s)
Bubble size	5.0 mm
Mesh size	10.0 mm
Time step	0.001 s

Fig. 5 shows the interaction of air bubbles (black) and sludge flocs (red) for the single plume and a bubble screen cases described above at two different simulation times, 7.5 (Fig. 5a) and 20 s (Fig. 5b). The sludge flocs are initially accumulated at the bottom quarter of the tank. These results depict the mechanisms of entrainment of inertial particles within the plume. For the single plume case (Fig. 5a), flocs are entrained from the bottom towards the centre of the plume and transported upwards; whenever the plume meandering drives these particles sideways, they will detrain and join the returning flow. Such

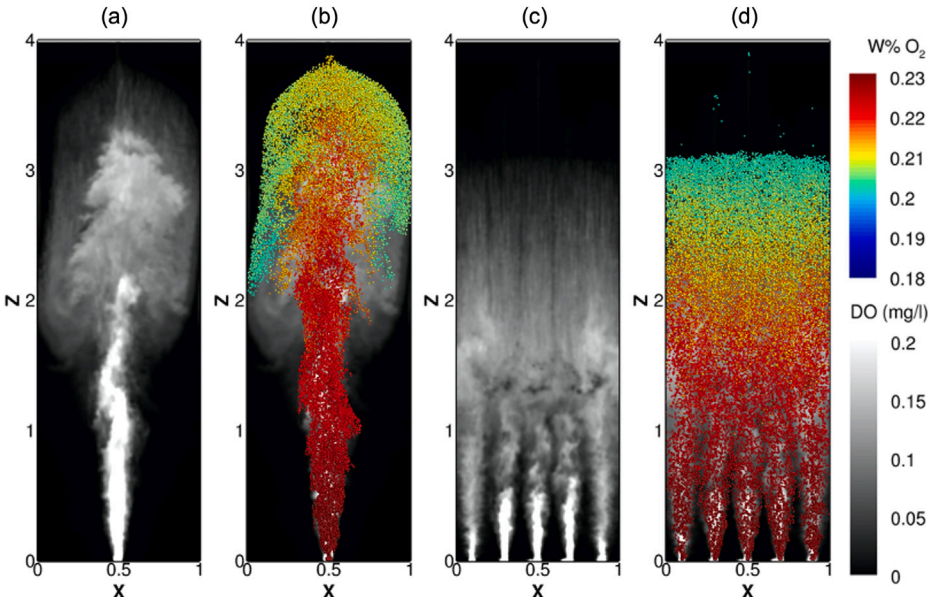

Fig. 4. Instantaneous distributions of (a) DO concentration and (b) O_2 mass fraction in air bubbles for a single plume; (c) DO concentration and (d) O_2 mass fraction in air bubbles for a bubble screen at early stages of the aeration. (For interpretation of the references to colour in this figure legend, the reader is referred to the web version of this article.)

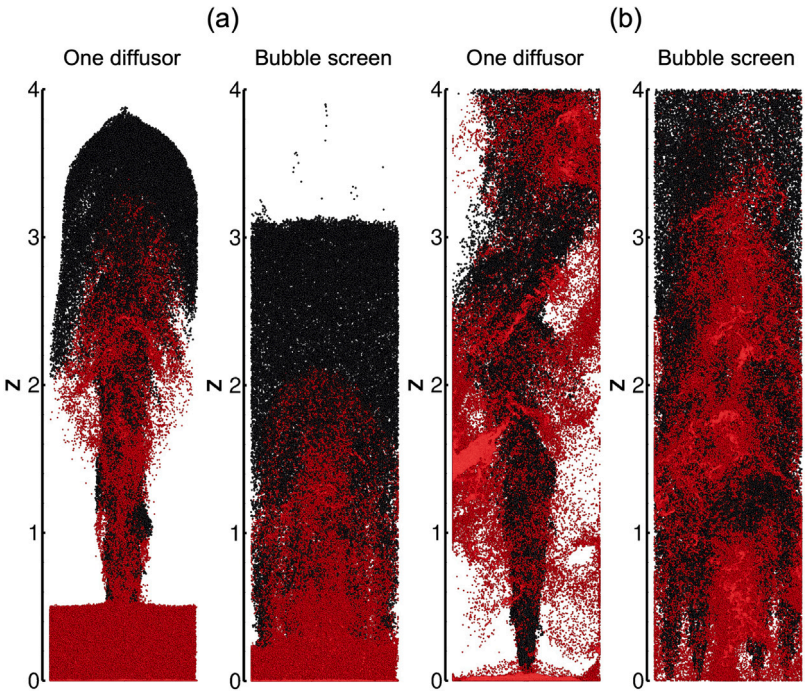

Fig. 5. Instantaneous Lagrangian fields of sludge particles (red) and air bubbles (black) for a single plume and a bubble screen at (a) 7.5 s and (b) 20 s into the simulation. (For interpretation of the references to colour in this figure legend, the reader is referred to the web version of this article.)

pattern is more evident 20 s into the simulation, depicted in Fig. 5b, where the bottom layer of settled particles has been almost completely sucked into the plume and there are several clusters of sludge flocs falling down. Such particles are not uniformly distributed, but shaped into patterns that replicate the vorticity induced by the plume in the surrounding fluid. In contrast, the bubble screen seems to entrain and detach particles more homogeneously. The inertial sludge flocs also seem to follow the turbulent structures triggered by the plumes as they fall, however such structures are smaller than in the single-plume case.

Fig. 6 represents the DO concentration and sludge volume fraction against the tank's depth at three different simulation times for the control case (bubble screen). The initial DO level is zero. Fig. 6a depicts a comparison between DO levels for clean water (no sludge) and wastewater, in which sludge is consuming Oxygen during its activation. As ASP progresses, oxygen is transferred from the air bubbles to the liquid starting near the bottom (5 s) but soon expanding towards the surface. The DO levels remain higher at the top of the tank due to the expansion of the plume and more bubbles being exposed to the water matrix. Clean water exhibits DO concentrations nearly 4 time higher than wastewater, albeit the patterns are very similar. This suggests that the mixing of particles is very effective and the uptake is nearly homogeneous throughout the tank, albeit more intense at the bottom. In fact, Fig. 6b quantifies the effectiveness of sludge mixing across the water column. The flocs originally settled at the bottom are

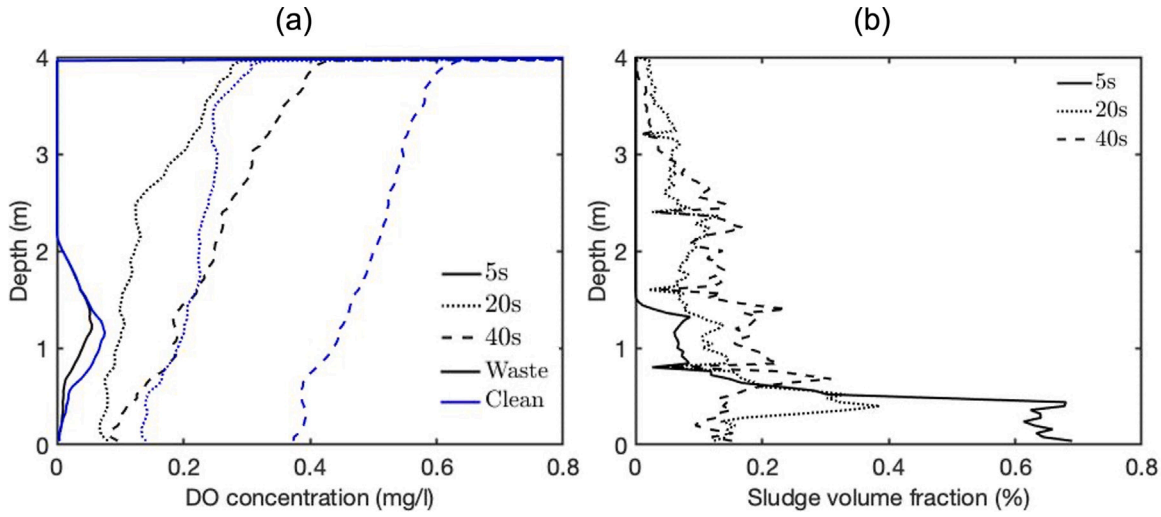

Fig. 6. DO and sludge volume fraction vertical profiles at three different simulation times (5, 20 and 40 s). Black lines: wastewater; blue lines: clean water. (For interpretation of the references to colour in this figure legend, the reader is referred to the web version of this article.)

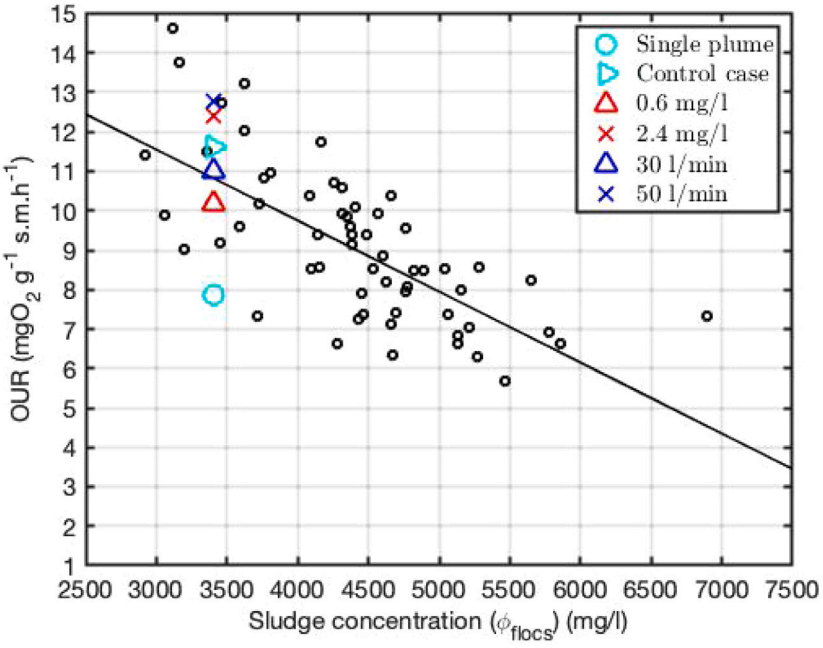

Fig. 7. Numerical-experimental comparison of sludge's oxygen uptake rate (Nowobilska-Majewska and Bugajski, 2020). (For interpretation of the references to colour in this figure legend, the reader is referred to the web version of this article.)

fairly well distributed within 20 s. The mixing never achieves complete homogeneity — the sludge concentration decreases with height due to the plume's buoyancy declining as the bubbles rise up and expand. Interestingly, however, the maximum sludge concentration after the very early stages of aeration is not at the bottom but around 0.75 m after 40 s. This could indicate an overall equilibrium between the plume's momentum and the flocs' inertia, similar to a lock-up height in stratified flows.

4.1. ASP model versus measurements

Fig. 7 presents a comparison of the Oxygen uptake rate (OUR) predicted by our ASP LES model (coloured symbols) and field measurements (circles) provided by Nowobilska-Majewska and Bugajski (2020) in different real-life wastewater treatment plants. The solid line describes the relation between OUR and sludge fraction discussed in Eq. (17). The numerical results correspond to five different cases, including the control case and four monoparametric variations of it: single-plume versus screen (light blue), lower and higher air flow rates (dark blue) and higher and lower initial DO levels (red). The entirety of our results fall within the experimental range for the same total sludge concentration. The three parameters explored show a significant impact on the Oxygen uptake levels. However, whilst a higher aeration rate or initial DO level can lead to approx. a 15% higher Oxygen uptake rate, aerator distributor seems to have a higher impact, with a difference around 30% in the OUR predicted for the single plume and the screen, in favour of the latter. This reinforces the pivotal role of homogeneous mixing in ASP.

4.2. Sensitivity analysis of ASP model

The response of our LES-based ASP model is analysed against a wide parameter range. The control scenario corresponds to the periodic tank shown in Fig. 3, bubble and sludge floc sizes 5 mm and 4.5 mm

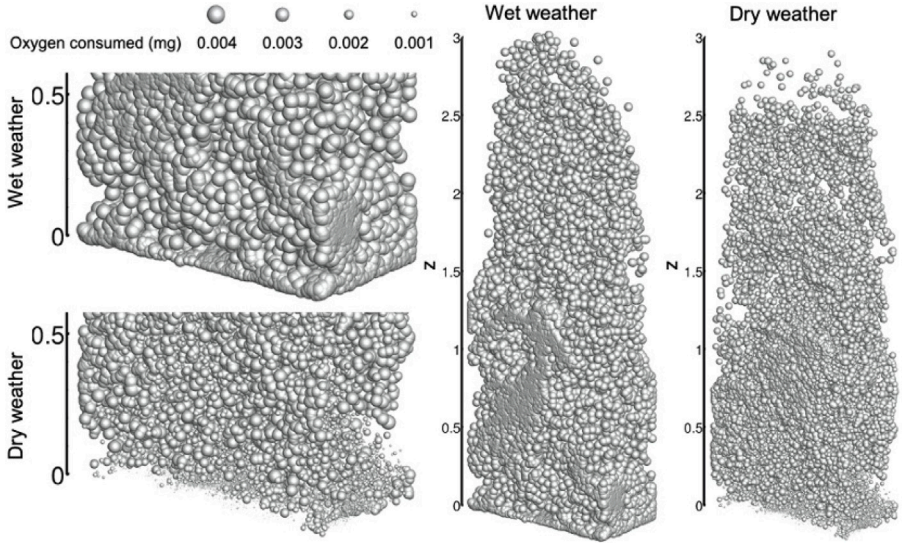

Fig. 8. Oxygen content of sludge particles at 8 s with DO_0 = 1.2 mg/l ('wet') and DO_0 = 0 mg/l ('dry').

Table 4
Parameter range tested with the ASP LES model.

Selected parameters	Value	Unit
Initial DO level	0.0 0.6, 1.2, 2.4	mg/l
Sludge floc size	4.0, 4.5, 5.5	mm
Air flow rate	30.0, 40.0, 50.0	l/min
Bubble size	4.0, 5.0, 6.0	mm

respectively, bubble-screen (5 cm gap between aerators) and 1.2 mg/l initial DO level. All remaining parameters are as described in Table 3. The physical parameters under analysis are (1) initial DO levels, (2) floc size, (3) air flow rate and (4) bubble size, as described in Table 4. For each analysis focused on one parameter, all remaining properties are as defined for the control scenario.

Initial DO levels are known to be relevant to ASP's performance and largely determined by atmospheric conditions. In very simplified terms, under 'dry' weather there is no oxygen dissolved in the water prior to aeration, since this has been all consumed by the sludge in the tank. However, rainfall ('wet' weather) promotes aeration at the tank's surface (Liu et al., 2020). Henceforth 'dry' designates zero initial DO levels in the tank and 'wet' a homogeneous initial distribution of DO_0 = 1.2 mg/l, unless stated otherwise. Fig. 8 reveals the influence of weather initial DO levels on sludge activation. The graphical representation of the floc size in the figure is a function of its individual oxygen consumption: larger particles have absorbed a larger O_2 content. Overall, the results show that the oxygen uptake under wet conditions is increased by approx. 100%; furthermore, the uptake range is narrowed from $10^{-3} - 2 \cdot 10^{-3}$ mg for dry, anoxic conditions to $3 \cdot 10^{-3} - 4 \cdot 10^{-3}$ mg in wet conditions. This is particularly noticeable at the tank's bottom, where the system struggles to bring DO when the initial levels are low.

The liquid phase, solved within the Eulerian framework, is the intermediary between the air bubbles and the sludge flocs in the oxygen transfer process. Fig. 9 shows isosurfaces of DO concentration at two different heights, z/H = 0.125 (left) and z/H = 0.625 (right), for the control case under wet (DO_0 = 1.2 mg/l) and dry (DO_0 = 0) conditions. The isosurfaces are colour-coded by the sludge volume fraction. The results demonstrate that initial DO levels are still critical after a long exposure to aeration. The left part of the figure corresponds to a location close to the bottom of the tank; the differences between 'dry' and 'wet' conditions are remarkable. When DO_0 = 0, the input from the bubble screen on the DO levels is revealed by the peaks aligned in the centreline of the computational domain, with the overall DO concentration being around 0.15 mg/l. In comparison, the wet scenario shows an overall slight decrease of the initial DO levels (DO_0 = 1.2 mg/l), with higher DO levels at the domain's corners; instead of the peaks observed in the dry case, there are deep cavities aligned with the centreline, that correspond to high concentrations of sludge absorbing the DO. This suggests that the DO levels in the dry case are too low to effectively activate the sludge particles near the bottom (in agreement with 8). The picture at $z/H = 0.625$ is rather different, in both cases there is a much more homogeneous mixture. There are still dips in at the centre of the domain for the wet case, although not as profound as near the bottom, revealing that the activation is intense, whereas the low DO levels in the dry case seem to constitute a bottleneck.

Fig. 10 shows time series of the oxygen transferred from bubbles (a) and oxygen uptake by sludge flocs (b) across the entire tank for two initial DO levels and diffuser setups (single plume and screen). The results regarding the bubble-to-liquid O_2 transfer show very similar trends across the parameter range. As previous results indicated, bubble screen ad lower DO_0 enhance bubble-to-liquid transfer. Interestingly, the effect of the bubble screen is sustained across the simulation time, i.e., it does not only contribute to increase the DO levels at the start of aeration. The higher Oxygen transfer achieved by the bubble screen is accumulative and does not hint to diminish during the initial 50 s of aeration. The analysis of the sludge uptake in Fig. 10b is more revealing of the mechanisms of activation. The initial DO levels determine the magnitude of sludge activation. Consistently with the previous results, the oxygen uptake by sludge is almost twice in wet conditions. There is also a different trend between wet and dry simulations at early stages ($t < 20$ s), due to the necessary build up of DO through aeration required under dry conditions to start the activation. The diffuser setup proves to be critical as well. The single plume case show a relaxation on the activation rate after 15 s; this is not observed for the bubble plume case. This can be attributed to the more effective mixing.

Fig. 11 adds sludge floc size influence into the analysis. The control scenario is tested with 4 mm, 4.5 mm and 5.5 mm monodispersed flocs in wet and dry weather. The total solid fraction in the tank was identical in all cases. The results reveal little response to the change in particle size, neither in magnitude nor trend. The influence of the initial DO level, however, is significant, particularly regarding Oxygen uptake by the sludge flocs. This suggests that the characteristic size of the flocs does not seem to have a significant impact on the physical processes taking place in the AS tank. However, it must be noted that we explored a small fraction of the parameter range, with floc sizes varying between

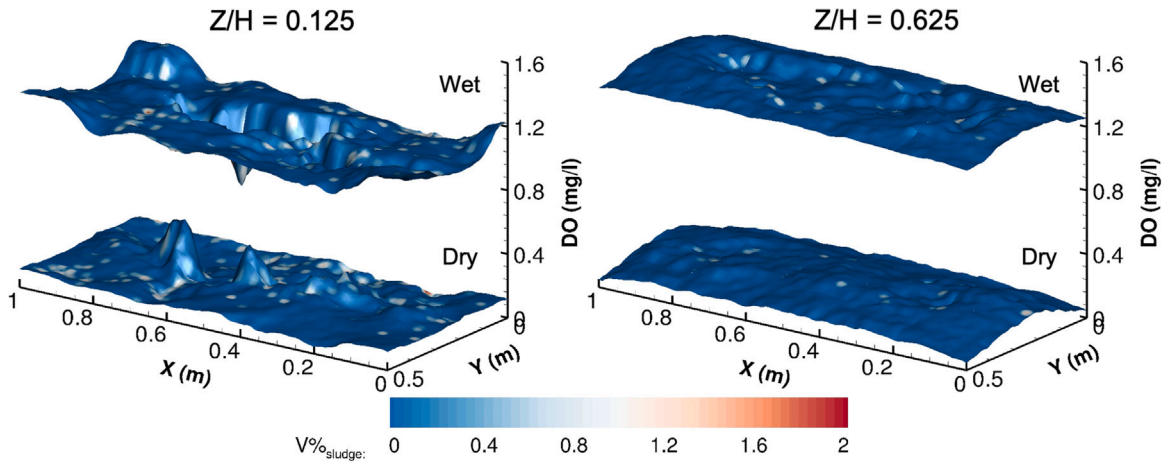

Fig. 9. Distribution of DO and sludge concentration for different wet ($DO_0 = 1.2$ mg/l) and dry ($DO_0 = 0$ mg/l) conditions: left, slice at $z/H = 0.125$; right, slice at $z/H = 0.625$. (For interpretation of the references to colour in this figure legend, the reader is referred to the web version of this article.)

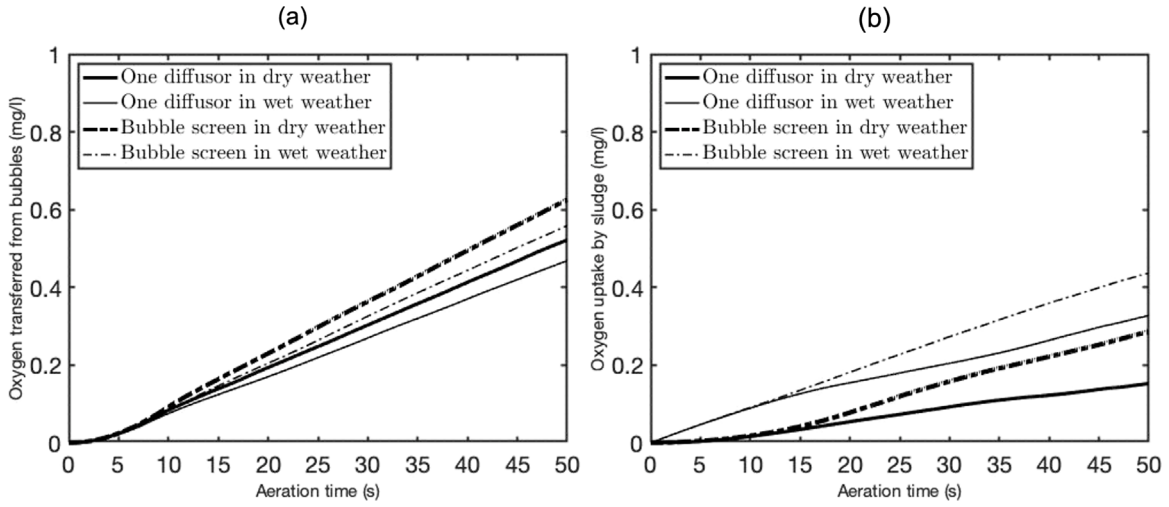

Fig. 10. Time evolution of oxygen transferred from bubbles to the wastewater (a) oxygen uptake by sludge flocs (b) across the computational domain for a single bubble plume and a bubble screen in wet and dry conditions.

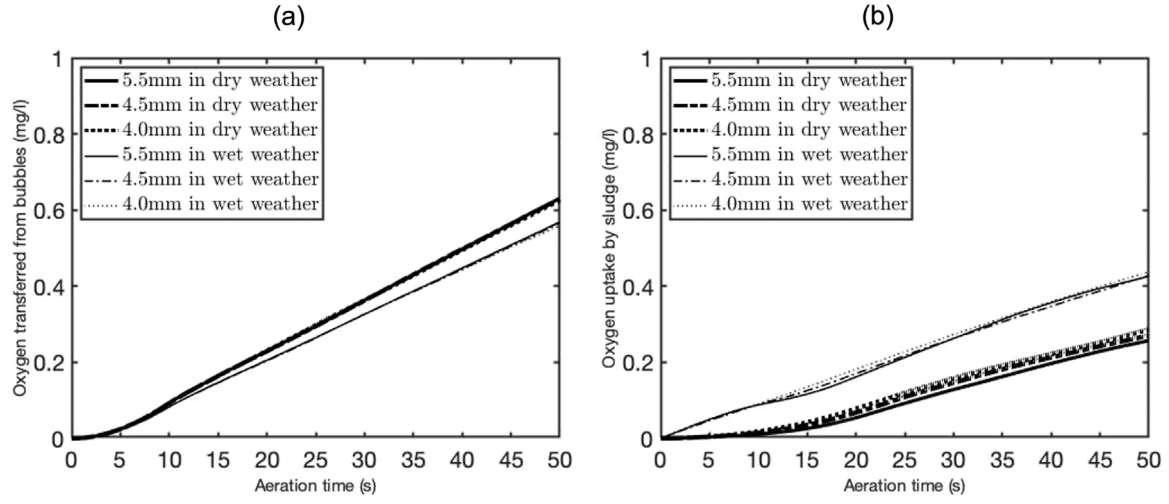

Fig. 11. Time evolution of oxygen transferred from bubbles to the wastewater (a) oxygen uptake by sludge flocs (b) across the computational domain for three different sludge sizes in wet and dry conditions.

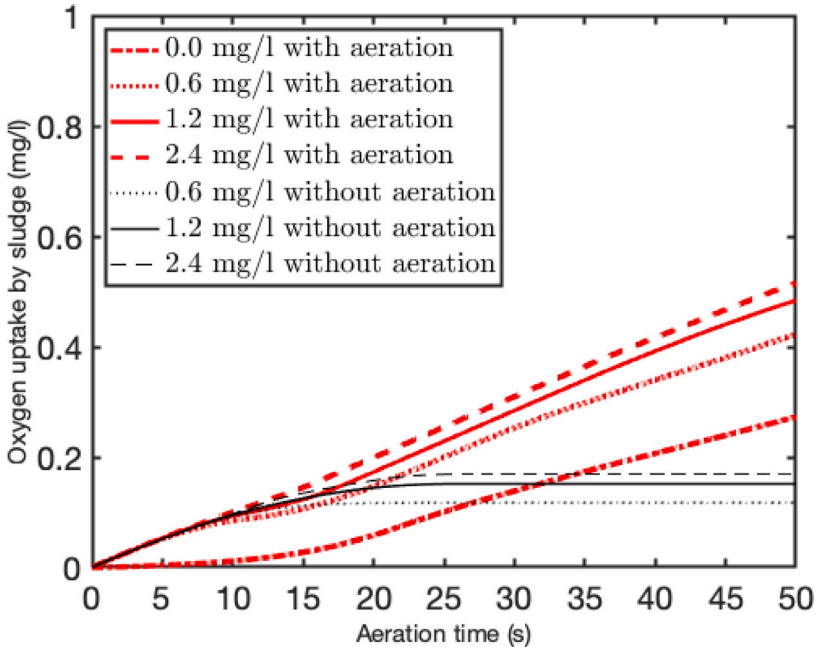

Fig. 12. Comparison of oxygen uptake by sludge for four different initial dissolved oxygen levels: 0, 0.6, 1.2 and 2.4 mg/l. Red thick lines: time evolution with aeration; Black thin lines: time evolution without aeration. (For interpretation of the references to colour in this figure legend, the reader is referred to the web version of this article.)

4 and 5.5 mm only. Within that range, the inertia of the solid phase appears not to be substantially changed. It is expected that increasing the floc size would reach a tipping point where the buoyant plumes would struggle to lift and entrain very large flocs. Our results suggest that below this critical size, the size (and, consequently, number) of flocs is not critical because it does not impede homogeneous mixing and aeration; and therefore its effect on ASP seems to be qualitative less relevant to the initial DO levels or the diffusers setup.

Fig. 12 explores further the sensitivity of to the initial DO levels considering four different values for DO_0: 0, 0.6, 1.2 and 2.4 mg/l. The plot illustrates the time evolution of the oxygen uptake by sludge flocs with and without aeration (i.e., no air bubbles). When aeration is present (red lines) DO_0 has a remarkable non-linear influence on sludge activation rate. Whereas $DO_0 = 0$ produces qualitatively worse rates of oxygen uptake, the differences between the other three levels are not that remarkable, despite DO_0 being increased a 100% at each step. As clearly illustrated by the cases without aeration, the initial DO levels will feed the ASP at early stages (roughly up to 10–15 s in this case), and the aeration assumes the role of main Oxygen provider from that point on, hence the flat line for the non-aerated cases. For aeration scenarios, lower initial DO levels result in a less smooth transition to bubbles being the source of DO. Interestingly, this impact seems to be long-lasting.

Fig. 13 shows time series of DO concentration recorded by two numerical probes located at 1 and 3.5 m along the central plane of the domain. In wet weather conditions ($DO_0 = 1.2$ mg/l), the lower probe reports a DO decline between 5 and 20 s. This corresponds to the time when the sludge particles reach that height and start consuming the available DO. After 20 s, aeration and activation reach an equilibrium and DO levels fluctuate around 1.1 mg/l. The upper probe reports a sustained DO increase, due to the lower presence of sludge (see Fig. 6) at that height and the inputs from air bubbles from approx. 10 s onwards. It is worth noting that the proximity to the free surface benefits from the atmospheric input, enhanced by the bubble plume-enhanced mixing. Regarding dry weather ($DO_0 = 0$), the overall DO concentration is approx. 80% lower than for wet conditions. Within that order of magnitude, the upper probe exhibits a similar trend to the one reported in the 'wet' case, with increasing DO due to aeration being dominant over aerobic digestion in sludge flocs. The lower probe does not measure DO levels increasing until over 20 s have passed either. During that period, the DO peaks generated by the aeration inputs are quickly consumed by the sludge. From 20 s onwards, an equilibrium appears to be also found in the dry case, with DO values fluctuating around 0.2 mg/l. These results emphasise the long-term effect of the initial DO levels in the tank.

Deciding on air flow rates constitutes one the main operational decisions in ASP. Fig. 14 quantitatively compares the integral amount of Oxygen absorbed by activated sludge under a range of conditions after 50 s of activation. Three gas flow rates (30, 40, 50 l/min) and three bubble sizes (4, 5, 6 mm) are examined. The amount of DO consumed per each sludge floc in the simulation was recorded, and the average μ_{O_2} and standard deviation σ_{O_2} calculated over a sample of 10^5 flocs across $5 \cdot 10^4$ timesteps. The ratio μ_{O_2}/σ_{O_2} is used as a quality indicator: a higher value indicates more DO uptake and more homogeneously distributed throughout the tank, and viceversa. Fig. 14a shows a significant gap depending on the initial DO levels, with μ_{O_2}/σ_{O_2} being on average 3 times higher in wet conditions. As expected, higher flow rates lead to higher ratios, and this trend appears to be non-linear. The μ_{O_2}/σ_{O_2} ratio for 50 l/min sees a nearly 40% increase when compared to 40 l/min. Fig. 14b shows the ratios for different bubble sizes (always under a constant flow rate), which can be controlled to a degree through the diffusers' design. The differences found are not significant, albeit the 5 mm bubbles provide the best results for the wet case, while 4 mm is better for the dry one, although virtually on pair with 5 mm. A smaller bubble size improves mass transfer by increasing the contact surface between phases, whereas larger bubbles provide wider buoyant plumes (Fraga and Stoesser, 2016), promoting a more homogeneous mixing.

5. Conclusions

This paper introduced the first three-dimensional LES-based model for activated sludge process (ASP) in wastewater treatment that accounts for the gas–liquid–solid interphase exchange of oxygen. A point-particle Eulerian–Lagrangian algorithm has been employed to investigate the three-phase flow encountered in ASP, with one continuous

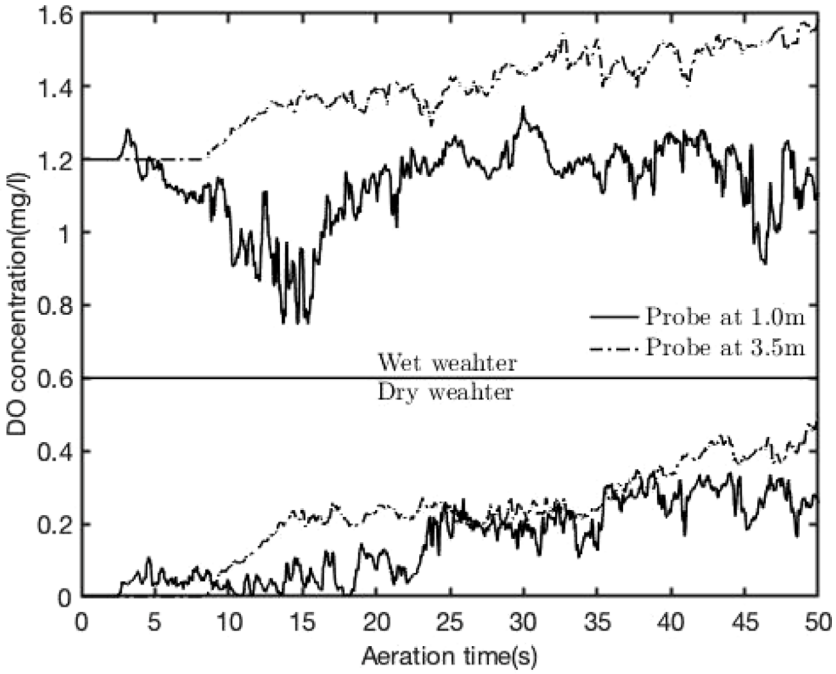

Fig. 13. Time evolution of DO concentration at two depths with different initial DO_0 = 1.2 mg/l (wet) and DO_0 = 0 (dry). Solid line: z = 1.0 m; dotted line: z = 3.5 m.

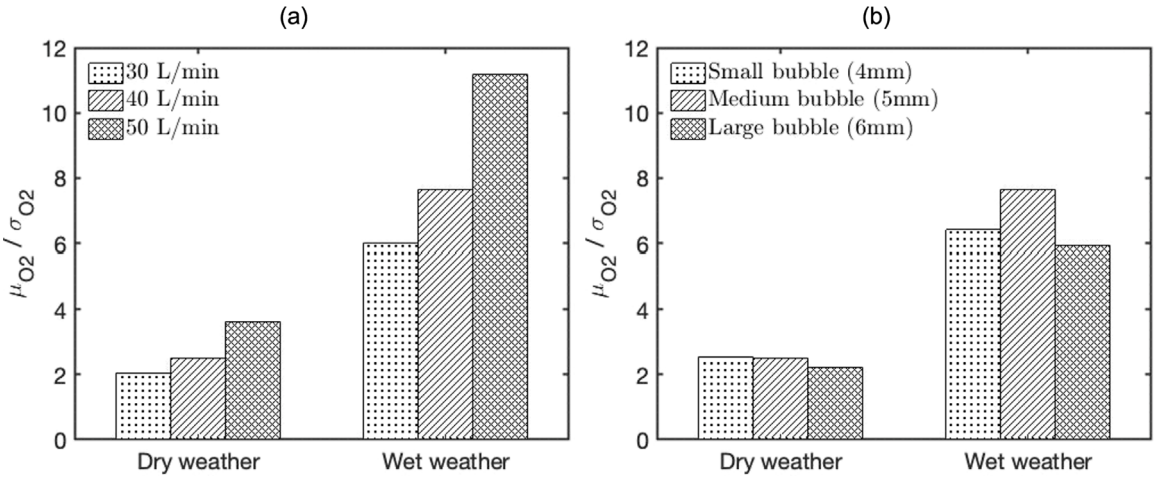

Fig. 14. Average versus standard deviation ratio of oxygen uptake by sludge flocs for different air flow rates (a) and bubble sizes (b).

phase (wastewater), one dispersed phase (air bubbles) and one non-Newtonian fluid (sludge) modelled by the coupled effect of discrete flocs and their effect on the surrounding water's viscosity according to its rheology. The model incorporates four-way coupling for the sludge flocs, allowing them to settle naturally and interact between each other following a soft-sphere collision model. The sources and sinks of dissolved oxygen were quantified at particle level. Basic physico-chemical kinetics were implemented to describe oxygen transfer from air bubbles and uptake by activated sludge. A pilot-scale bubble reactor was modelled to validate the ability of the solver to predict oxygen transfer from air bubbles to water versus experimental measurements (McClure et al., 2018), exhibiting a remarkable agreement at five different superficial gas velocities and a qualitatively better performance than prior Eulerian–Eulerian RANS-based simulations.

The LES-based ASP model was then tested under realistic operating conditions in a wastewater facility within a periodic domain. The ability of the model to predict oxygen consumption by sludge was compared to measurements obtained in wastewater plants, falling clearly within the experimental range. The turbulence-resolving nature of the simulations provided insights on the fluid dynamics involved on the interaction between phases, including the dual role of aeration on ASP. Firstly, air bubbles provide a source of oxygen. Our results showed that air bubbles in the outer regions of the plume were able to effectively transfer oxygen, whereas those at the plume's core remained shielded in an high-speed, oxygen-rich region and therefore are rather ineffective. Consequently, increasing the number of aerators (at a constant air flow rate) maximises the air bubble exposure and contributes to higher levels of dissolved oxygen across the tank. Secondly, air bubbles trigger turbulent mixing that is extremely effective redistributing sludge within the domain; our simulations showed how sludge flocs are entrained by the buoyant plumes and then detached following transient meandering patterns.

It was noted that the initial DO levels in the tank controlled the activation's rate, whereas the diffuser distribution rules its evolution in time. Low DO levels before aeration starts have a long lasting effect, acting as a limiting factor for ASP. High initial DO levels increase by at least 100% the overall ASP performance when compared to anoxic conditions. It must be however noted that the increased performance

decays gradually as the initial DO levels approach saturation. This parameter does not only affect the total oxygen consumed by activated sludge, but also the homogeneity of the aerobic digestion in the tank. Homogeneity is key to achieve a global equilibrium between aeration and activation and avoiding build up of anoxic layers or well-aerated regions without sludge. Another key parameter is the air flow rate, whose increase results in a non-linear improvement of the overall activation performance. On the other hand, floc and bubble size were found to be relatively irrelevant on the overall process.

Declaration of competing interest

The authors declare that they have no known competing financial interests or personal relationships that could have appeared to influence the work reported in this paper.

Data availability

No data was used for the research described in the article.

Acknowledgements

The computational work described in this paper was performed using the University of Birmingham BlueBEAR HPC service and HPC Midlands+. The authors are grateful for the support provided by the University and EPSRC.

References

Baker, M.C., Kong, B., Capecelatro, J., Desjardins, O., Fox, R.O., 2020. Direct comparison of Eulerian–Eulerian and Eulerian–Lagrangian simulations for particle-laden vertical channel flow. AIChE J. 66 (7), e16230.
Balachandar, S., Eaton, J.K., 2010. Turbulent dispersed multiphase flow. Annu. Rev. Fluid Mech. 42, 111–133.
Bini, M., Jones, W., 2008. Large-eddy simulation of particle-laden turbulent flows. J. Fluid Mech. 614, 207–252.
Bridgeman, J., 2012. Computational fluid dynamics modelling of sewage sludge mixing in an anaerobic digester. Adv. Eng. Softw. 44 (1), 54–62.
Brouckaert, C., Buckley, C., 1999. The use of computational fluid dynamics for improving the design and operation of water and wastewater treatment plants. Water Sci. Technol. 40 (4–5), 81–89.
Buwa, V.V., Deo, D.S., Ranade, V.V., 2006. Eulerian–Lagrangian simulations of unsteady gas–liquid flows in bubble columns. Int. J. Multiph. Flow. 32 (7), 864–885.
Cantero, M.I., Balachandar, S., Garcia, M.H., 2008. An Eulerian–Eulerian model for gravity currents driven by inertial particles. Int. J. Multiph. Flow. 34 (5), 484–501.
Capecelatro, J., Desjardins, O., 2013. An Euler–Lagrange strategy for simulating particle-laden flows. J. Comput. Phys. 238, 1–31.
Cevheri, M., Stoesser, T., 2018. Large-eddy simulation of a jet in crossflow using local mesh refinement. Prog. Comput. Fluid Dyn., Int. J. 18 (3), 137–149.
Chen, B., Fraga, B., Hemida, H., 2021. Large-eddy simulation of enhanced mixing with buoyant plumes. Chem. Eng. Res. Des..
Cundall, P.A., Strack, O.D., 1979. A discrete numerical model for granular assemblies. Geotechnique 29 (1), 47–65.
Dapelo, D., Alberini, F., Bridgeman, J., 2015. Euler-Lagrange CFD modelling of unconfined gas mixing in anaerobic digestion. Water Res. 85, 497–511.
Darmana, D., Deen, N., Kuipers, J., 2005. Detailed modeling of hydrodynamics, mass transfer and chemical reactions in a bubble column using a discrete bubble model. Chem. Eng. Sci. 60 (12), 3383–3404.
Deen, N.G., van Sint Annaland, M., Kuipers, J., 2004. Multi-scale modeling of dispersed gas–liquid two-phase flow. Chem. Eng. Sci. 59 (8–9), 1853–1861.
Dhotre, M.T., Niceno, B., Smith, B.L., Simiano, M., 2009. Large-eddy simulation (LES) of the large scale bubble plume. Chem. Eng. Sci. 64 (11), 2692–2704.
Elghobashi, S., 1994. On predicting particle-laden turbulent flows. Appl. Sci. Res. 52 (4), 309–329.
Eshtiaghi, N., Markis, F., Yap, S.D., Baudez, J.-C., Slatter, P., 2013. Rheological characterisation of municipal sludge: a review. Water Res. 47 (15), 5493–5510.
Fabregat, A., Dewar, W.K., Özgökmen, T.M., Poje, A.C., Wienders, N., 2015. Numerical simulations of turbulent thermal, bubble and hybrid plumes. Ocean Model. 90, 16–28.
Fernández, F., Castro, M., Rodrigo, M., Cañizares, P., 2011. Reduction of aeration costs by tuning a multi-set point on/off controller: A case study. Control Eng. Pract. 19 (10), 1231–1237.
Forster, C.F., 2002. The rheological and physico-chemical characteristics of sewage sludges. Enzyme Microb. Technol. 30 (3), 340–345.
Forster, C.F., 2003. Wastewater Treatment and Technology. Thomas Telford.
Fraga, B., Stoesser, T., 2016. Influence of bubble size, diffuser width, and flow rate on the integral behavior of bubble plumes. J. Geophys. Res.: Oceans 121 (6), 3887–3904.
Fraga, B., Stoesser, T., Lai, C.C., Socolofsky, S.A., 2016. A LES-based Eulerian–Lagrangian approach to predict the dynamics of bubble plumes. Ocean Model. 97, 27–36.
Hryb, D., Cardozo, M., Ferro, S., Goldschmit, M., 2009. Particle transport in turbulent flow using both Lagrangian and Eulerian formulations. Int. Commun. Heat Mass Transfer 36 (5), 451–457.
Hu, G., Celik, I., 2008. Eulerian–Lagrangian based large-eddy simulation of a partially aerated flat bubble column. Chem. Eng. Sci. 63 (1), 253–271.
Huang, Y., Yang, C., Wen, C., Wen, G., 2019. S-type dissolved oxygen distribution along water depth in a canyon-shaped and algae blooming water source reservoir: reasons and control. Int. J. Environ. Res. Public Health 16 (6), 987.
Karpinska, A.M., Bridgeman, J., 2016. CFD-aided modelling of activated sludge systems–A critical review. Water Res. 88, 861–879.
Karpinska, A.M., Dias, M.M., Boaventura, R.A., Santos, R.J., 2015. Modeling of the hydrodynamics and energy expenditure of oxidation ditch aerated with hydrojets using CFD codes. Water Qual. Res. J. Can. 50 (1), 83–94.
Kartushinsky, A., Tisler, S., Oliveira, J.G., Van der Geld, C., 2016. Eulerian-Eulerian modelling of particle-laden two-phase flow. Powder Technol. 301, 999–1007.
Lai, C., Fraga, B., Chan, W., Dodd, M., 2018. Energy cascade in a homogeneous swarm of bubbles rising in a vertical channel. In: Proceedings of the Summmer Program.
Le Moullec, Y., Gentric, C., Potier, O., Leclerc, J., 2010. CFD simulation of the hydrodynamics and reactions in an activated sludge channel reactor of wastewater treatment. Chem. Eng. Sci. 65 (1), 492–498.
Li, G., Yang, X., Dai, G., 2009. CFD simulation of effects of the configuration of gas distributors on gas–liquid flow and mixing in a bubble column. Chem. Eng. Sci. 64 (24), 5104–5116.
Link, J., Cuypers, L., Deen, N., Kuipers, J., 2005. Flow regimes in a spout–fluid bed: A combined experimental and simulation study. Chem. Eng. Sci. 60 (13), 3425–3442.
Liu, Y., Du, J., Hu, P., Ma, M., Hu, D., 2020. Microtopographic modification conserves urban wetland water quality by increasing the dissolved oxygen in the wet season. J. Environ. Sci. 87, 71–81.
Lu, J., Fernández, A., Tryggvason, G., 2005. The effect of bubbles on the wall drag in a turbulent channel flow. Phys. Fluids 17 (9), 095102.
Magolan, B., Lubchenko, N., Baglietto, E., 2019. A quantitative and generalized assessment of bubble-induced turbulence models for gas-liquid systems. Chem. Eng. Sci.: X 2, 100009.
Maktabifard, M., Zaborowska, E., Makinia, J., 2018. Achieving energy neutrality in wastewater treatment plants through energy savings and enhancing renewable energy production. Rev. Environ. Sci. Bio/Technol. 17 (4), 655–689.
McClure, D.D., Liu, Z., Barton, G.W., Fletcher, D.F., Kavanagh, J.M., 2018. Oxygen transfer in pilot-scale contactors: An experimental and computational investigation into the effect of contactor design. Chem. Eng. J. 344, 173–183.
Mehrabadi, M., Horwitz, J., Subramaniam, S., Mani, A., 2018. A direct comparison of particle-resolved and point-particle methods in decaying turbulence. J. Fluid Mech. 850, 336–369.
Motarjemi, M., Jameson, G., 1978. Mass transfer from very small bubbles—the optimum bubble size for aeration. Chem. Eng. Sci. 33 (11), 1415–1423.
Nasr-Azadani, M., Hall, B., Meiburg, E., 2013. Polydisperse turbidity currents propagating over complex topography: comparison of experimental and depth-resolved simulation results. Comput. Geosci. 53, 141–153.
Nowobilska-Majewska, E., Bugajski, P., 2020. The impact of selected parameters on the condition of activated sludge in a biologic reactor in the treatment plant in nowy targ, Poland. Water 12 (10), 2657.
Ouro, P., Fraga, B., Lopez-Novoa, U., Stoesser, T., 2019. Scalability of an Eulerian-Lagrangian large-eddy simulation solver with hybrid MPI/OpenMP parallelisation. Comput. & Fluids 179, 123–136.
Ouro, P., Fraga, B., Viti, N., Angeloudis, A., Stoesser, T., Gualtieri, C., 2018. Instantaneous transport of a passive scalar in a turbulent separated flow. Environ. Fluid Mech. 18 (2), 487–513.
Paul, I., Fraga, B., Dodd, M.S., Lai, C., 2022. The role of breakup and coalescence in fine-scale bubble-induced turbulence. I. Dynamics. Phys. Fluids 34 (8), 083321.
Pryamitsyn, V., Ganesan, V., 2006. Mechanisms of steady-shear rheology in polymer-nanoparticle composites. J. Rheol. 50 (5), 655–683.
Rieger, L., Alex, J., Gujer, W., Siegrist, H., 2006. Modelling of aeration systems at wastewater treatment plants. Water Sci. Technol. 53 (4–5), 439–447.
Sánchez, F., Rey, H., Viedma, A., Nicolás-Pérez, F., Kaiser, A., Martínez, M., 2018. CFD simulation of fluid dynamic and biokinetic processes within activated sludge reactors under intermittent aeration regime. Water Res. 139, 47–57.
Sánchez-Monedero, M., Aguilar, M., Fenoll, R., Roig, A., 2008. Effect of the aeration system on the levels of airborne microorganisms generated at wastewater treatment plants. Water Res. 42 (14), 3739–3744.
Sander, R., 2015. Compilation of Henry's law constants (version 4.0) for water as solvent. Atmos. Chem. Phys. 15 (8), 4399–4981.
Smith, H.S., 1963. Oxygen Uptake in a Completely Mixed Activated Sludge System (Ph.D. thesis).

Sokolichin, A., Eigenberger, G., Lapin, A., Lübert, A., 1997. Dynamic numerical simulation of gas-liquid two-phase flows Euler/Euler versus Euler/Lagrange. Chem. Eng. Sci. 52 (4), 611–626.

Terashima, M., Goel, R., Komatsu, K., Yasui, H., Takahashi, H., Li, Y., Noike, T., 2009. CFD simulation of mixing in anaerobic digesters. Bioresour. Technol. 100 (7), 2228–2233.

Vui Chua, K., Fraga, B., Stoesser, T., Ho Hong, S., Sturm, T., 2019. Effect of bridge abutment length on turbulence structure and flow through the opening. J. Hydraul. Eng. 145 (6), 04019024.

Wilén, B.-M., Balmér, P., 1998. Short term effects of dissolved oxygen concentration on the turbidity of the supernatant of activated sludge. Water Sci. Technol. 38 (3), 25–33.

Wilén, B.-M., Balmér, P., 1999. The effect of dissolved oxygen concentration on the structure, size and size distribution of activated sludge flocs. Water Res. 33 (2), 391–400.

Xie, H., Yang, J., Hu, Y., Zhang, H., Yang, Y., Zhang, K., Zhu, X., Li, Y., Yang, C., 2014. Simulation of flow field and sludge settling in a full-scale oxidation ditch by using a two-phase flow CFD model. Chem. Eng. Sci. 109, 296–305.

Yujie, Z., Mingyan, L., Yonggui, X., Can, T., 2012. Three-dimensional volume of fluid simulations on bubble formation and dynamics in bubble columns. Chem. Eng. Sci. 73, 55–78.

Zhou, Z., Huang, T., Gong, W., Li, Y., Liu, Y., Zhou, S., Cao, M., 2019. Water quality responses during the continuous mixing process and informed management of a stratified drinking water reservoir. Sustainability 11 (24), 7106.